Taylor & Francis
Taylor & Francis Group

BRIEF REPORT

OPEN ACCESS | Check for updates

Investigation of the enantioselectivity of acetylcholinesterase and butyrylcholinesterase upon inhibition by tacrine-iminosugar heterodimers

I. Caroline Vaaland[a], Óscar López[b] (iD), Adrián Puerta[c] (iD), Miguel X. Fernandes[c] (iD), José M. Padrón[c] (iD), José G. Fernández-Bolaños[b] (iD), Magne O. Sydnes[a] (iD) and Emil Lindbäck[a] (iD)

aDepartment of Chemistry, Bioscience and Environmental Engineering, Faculty of Science and Technology, University of Stavanger, Stavanger, Norway; bDepartamento de Química Orgánica, Facultad de Química, Universidad de Sevilla, Seville, Spain; cBioLab, Instituto Universitario de Bio-Orgánica "Antonio González" (IUBO-AG), Universidad de La Laguna, c/Astrofísico Francisco Sánchez, La Laguna, Spain

ABSTRACT

The copper-catalysed azide-alkyne cycloaddition was applied to prepare three enantiomeric pairs of heterodimers containing a tacrine residue and a 1,4-dideoxy-1,4-imino-D-arabinitol (DAB) or 1,4-dideoxy-1,4-imino-L-arabinitol (LAB) moiety held together via linkers of variable lengths containing a 1,2,3-triazole ring and 3, 4, or 7 CH_2 groups. The heterodimers were tested as inhibitors of butyrylcholinesterase (BuChE) and acetylcholinesterase (AChE). The enantiomeric heterodimers with the longest linkers exhibited the highest inhibition potencies for AChE ($IC_{50} = 9.7$ nM and 11 nM) and BuChE ($IC_{50} = 8.1$ nM and 9.1 nM). AChE exhibited the highest enantioselectivity (ca. 4-fold). The enantiomeric pairs of the heterodimers were found to be inactive ($GI_{50} > 100\,\mu M$), or to have weak antiproliferative properties ($GI_{50} = 84–97\,\mu M$) against a panel of human cancer cells.

Introduction

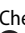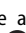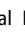Enzyme inhibition represents an attractive target for drug development[1]. Because enzymes are built up by chiral building blocks, amino acids, it is not surprising if only one member of an enantiomeric pair causes inhibition upon binding. Another alternative is that both enantiomers display various degrees of inhibition, due to different interaction modes[2–4]. One such example is the natural enantiomer 1a (Figure 1) of huperzine A, which is a 38- to 49-fold more potent AChE inhibitor than its unnatural enantiomer 1b[5,6]. In fact, inhibition of cholinesterases (ChEs) is an attractive target for treatment of Alzheimer's disease (AD) and there are currently three ChE inhibitors on the list of FDA approved AD drugs[7]. (–)-Huperzine (1a) is not on the list of FDA approved drugs, but it was approved in China as a symptomatic AD drug[8,9]. The much stronger AChE inhibition exhibited by 1a compared to 1b, was partially rationalised by comparison of the X-ray structures of Torpedo californica acetylcholinesterase (TcAChE) complexed with enantiomers 1a and 1b, which demonstrated the presence and absence of an interaction between the ethylidene methyl of 1a and 1b, respectively, with His440[10], which is a member of the catalytic triad almost on the bottom of a ca. 20 Å deep active gorge of TcAChE[11].

(–)-Galantamine (2a) (Figure 1) is an FDA approved ChE inhibitor drug for the treatment of mild-to-moderate AD[7]. This alkaloid is a reversible AChE inhibitor and exhibits 53-times selectivity for AChE over BuChE[12]. X-ray studies of the TcAChE/(-)-galantamine complex revealed that the inhibitor binds in its acidic form at the base of the active gorge in the region between the acetyl hole

and the catalytic anionic site (CAS)[13]. The protonated amine group is quite remote from Trp84 in CAS and thereby is not involved in any cation–π interactions with the Trp84 residue, which is in stark contrast to acetylcholine (ACh), whose quaternary ammonium group establishes a cation–π interaction with Trp84. Instead, the high affinity of (-)-galantamine for AChE was attributed to multiple moderate and weak interactions with the enzyme[13]. The inhibition of AChE by galantamine appears to be enantioselective, at 20 μM inhibitor concentration, as the natural enantiomer 2a (ca. 94% of inhibition) is a much stronger inhibitor than its unnatural antipode 2b (ca. 4% of inhibition)[14], which indicates that several interactions with the enzyme are eliminated or attenuated when the configuration in all stereogenic centres of 2a is reversed.

Significant enantioselectivity has also been observed for the inhibition of AChE by physostigmine; natural (-)-physostigmine (3a) (Figure 2) is a ca. 25- to 1000-fold stronger inhibitor, depending on the enzyme source, than (+)-physostigmine (3b)[15,16].

Iminosugars are glycomimetics in which the ring oxygen atom has been replaced by a nitrogen atom[17]. Iminosugars are attractive as pharmaceutical candidates because they inhibit glycosidases without being metabolised by such enzymes[18]. Such properties have made iminosugars attractive as synthetic targets[19] and lead compounds for the treatment of various diseases such as viral infections, diabetes, type 2 diabetes, and lysosomal disorders[20]. In addition, it has been found that iminosugars are able to inhibit the growth of cancer cells[21,22], without affecting the viability and mortality of normal cells[21]. To date, three iminosugars, namely, miglitol[23], miglustat[24], and migalastat[25] have been approved by
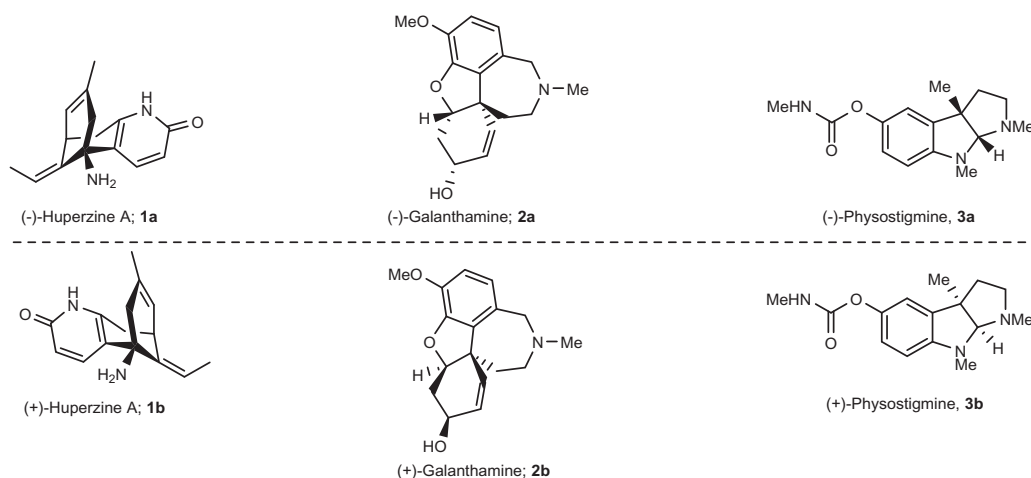
Figure 1. Examples of enantiomeric pairs of ChE inhibitors of which the mirror images display different potencies.
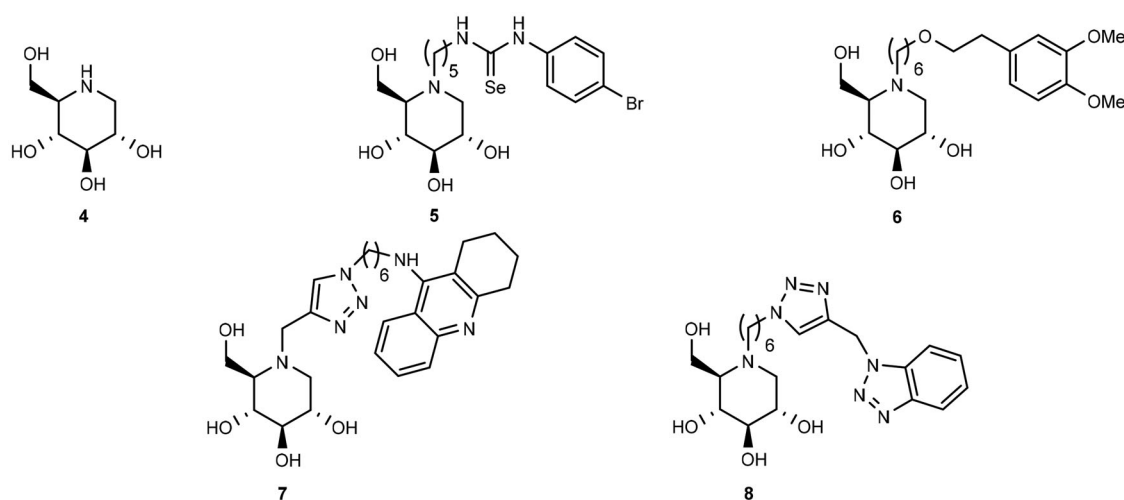

Figure 2. Selected examples of iminosugars that have been investigated as ChE inhibitors.

FDA for the treatment of type 2 diabetes, Gaucher's disease, and Fabry's disease, respectively. Miglustat has also been found to reduce the production of amyloid β-peptide (Aβ)[26], which is a component of senile plaque in AD patients.

The ester group of ACh is held in place for hydrolysis by the catalytic triad in the active gorge of AChE by the aid of cation $-\pi$ interactions with a Trp residue in CAS[27]. Because many iminosugars are protonated at physiological pH[28], they were proposed to be capable of inhibiting ChEs[29]. Thereby, a series of iminosugars of various stereochemistry and substitution patterns have been tested as ChE inhibitors, displaying particularly good BuChE inhibition[29]. Following this line, some of us have reported the synthesis and ChE inhibitory testing of bivalent inhibitors in which a 1-deoxynojirimycin (1-DNJ) (**4**) binding unit is connected to a second binding unit, namely, aryl-substituted selenourea (exemplified by **5**)[30], catechol (exemplified by **6**)[31], tacrine (exemplified by **7**)[32], or benzotriazole (exemplified by **8**)[33] binding unit (Figure 2). Kinetic assays and modelling studies for the binding of **6**, **7**, and **8** to AChE indicated that they behave as dual binding site AChE inhibitors, which implies that they bind simultaneously to the peripheral anionic site (PAS) and CAS. A more surprising observation (given that the quaternary ammonium group of ACh participates in a cation–π interaction with a Trp residue in CAS) from the modelling studies was that when heterodimers **6** and **8** bind to AChE in their protonated states (on the 1-DNJ nitrogen atom), the positive

charged nitrogen atom is not necessarily involved in cation $-\pi$ interactions with the aromatic residues of the enzyme[31,33].

Thus far, five papers have been published, which demonstrate the potential of iminosugars as ChE inhibitors[29–33]. One entry of ChE inhibition by iminosugars that remains to be studied is whether iminosugars can achieve enantioselective ChE inhibition. Thus, in this paper, we present the synthesis of three pairs of optically pure iminosugar-tacrine heterodimer enantiomers, namely, **9a** and **9b**, **10a** and **10b**, and **11a** and **11b** (Scheme 1) and the evaluation of their performance as ChE inhibitors. The study also includes docking studies of the heterodimers to predict interaction with AChE and BuChE. Naturally occurring 1,4-dideoxy-1,4-imino-D-arabinitol (DAB) (**12a**) constitutes the iminosugar moiety in **9a**, **10a**, and **11a**, whereas non-natural 1,4-dideoxy-1,4-imino-L-arabinitol (LAB) (**12b**) is the iminosugar moiety in **9b**, **10b**, and **11b**. Because both iminosugars[21,22], and heterodimers containing a tacrine moiety[34] have been found to inhibit the growth of cancer cells, we also report the antiproliferative screening of **11a** and **11b** against a panel of six cancer cell lines.

Materials and methods

General procedures

Dichloromethane (DCM), methanol (MeOH), acetone, dimethyl sulfoxide (DMSO) and dimethylformamide (DMF) were dried over 4 Å
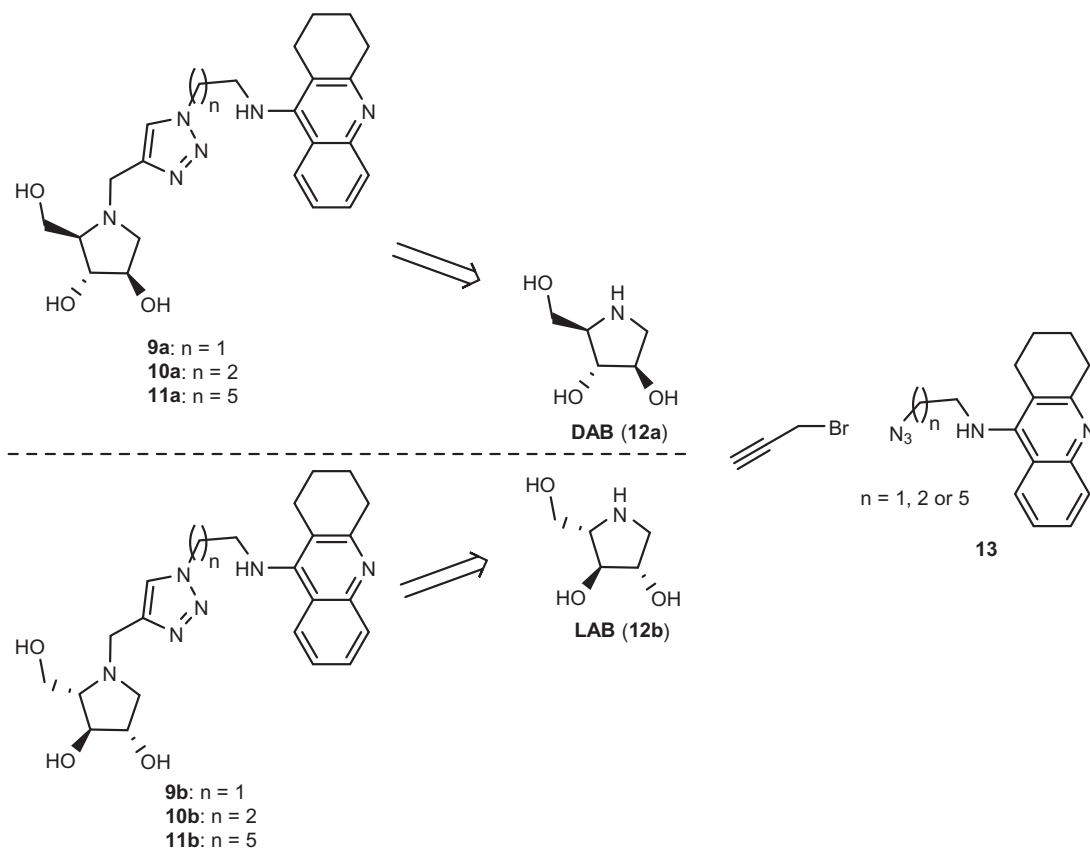
Scheme 1. Retrosynthetic pathways to the optically pure pairs of enantiomers **9a** and **9b**, **10a** and **10b**, and **11a** and **11b**.

molecular sieves (oven dried). Petroleum ether (PE) from the 40–65 °C fraction was used for silica flash columns. All reactions were carried out under Ar atmosphere if not otherwise specified. Reactions performed at room temperature (rt) refer to the temperature range of 20 to 22 °C. TLC analyses were performed on Merck silica gel 60 F_{254} plates using UV light ($\lambda = 254$ nm) for detection. Silica gel NORMASIL 60® 40–63 μm was used for silica flash columns. A Bruker Avance NMR spectrometer was used to record ^{1}H-NMR spectra (400.13 MHz) and ^{13}C-NMR spectra (100.61 MHz) in CDCl₃, CD₃OD, or D₂O. Chemical shifts (δ) are reported relative to residual DMSO (δ 2.50 ppm, ^{1}H; δ 39.52 ppm, ^{13}C), residual CHCl₃ in CDCl₃ (δ 7.26 ppm, ^{1}H; δ 77.16 ppm, ^{13}C), residual CD₃OD (δ 3.31 ppm, ^{1}H; δ 49.0 ppm, ^{13}C), residual D₂O (δ 4.79 ppm, ^{1}H) and TMS as an internal standard in CDCl₃. High-resolution mass spectra (HRMS) were recorded on a Qexactive spectrometer in positive electrospray ionisation (ESI) mode.

Synthetic protocols
General procedure for the preparation of compounds 20a–22a and 20b–22b. A mixture of **19b** (1 equiv., 0.04 M for synthesis of **20b**, **21b**, and **22b**) or **19a** (1 equiv., 0.07 M for synthesis of **20a**, 0.04 M for synthesis of **21a**, and 0.05 M for synthesis of **22a**), azide **13** (0.98 equiv.), and copper(II) sulphate pentahydrate (0.30 equiv.) in anhydrous DMF in an aluminium foil covered round bottom flask was degassed and introduced an argon atmosphere before the addition of sodium ascorbate (0.60 equiv.). After addition, the mixture was kept stirring for 48 h at rt. The solvent was then removed under reduced pressure and the residue obtained was

purified by silica gel column chromatography (See Supplementary Material for details).

General procedure for the preparation of compounds 9a–11a and 9b–11b. To a mixture of **20a–22a** (0.02 M, 1 equiv.) or **20b–22b** (0.02 M, 1 equiv.) in anhydrous CH₂Cl₂ under an argon atmosphere at −78 °C was slowly added BCl₃ (1 M in heptane, 15 equiv.). After addition, the mixture was kept stirring at −78 °C for 2 h and then at 0 °C overnight. The volatiles were then removed under reduced pressure and the concentrate underwent purification by gradient silica gel chromatography (MeCN/H₂O/NH₄OH 190:10:1 → 180:20:1) (column 1). The corresponding HCl salt was dissolved in MeOH (2 ml) and NH₄OH (0.5 ml) and kept stirring for 48 h. The solvent was removed under reduced pressure and the resulting residue was purified by gradient silica gel chromatography (column 2) (the solvent gradient for column 2 for each single experiment is specified in the Supplementary Material).

Inhibition assays
Measuring of the inhibition activity of compounds **9a–11a** and **9b–11b** against cholinesterases (AChE from *Electrophorus electricus* and BuChE from equine serum) was accomplished following minor modifications of the Ellman assay[35], as reported previously[36]. A Thermo Scintific™ Varioskan™ LUX microplate reader and Greiner F-bottom 96-well plates were used. Cornish-Bowden plots (1/V *vs.* [I] and [S]/V *vs.* [I]) were used for the visualisation of the mode of inhibition. Calculation of the kinetic parameters (K_M, V_{max}) was accomplished using a nonlinear regression analysis (least squares

fit) implemented in GraphPad Prism 8.01 software; such parameters were in turn used for calculating the inhibition constants of the mixed inhibitors using the following equations:

$$K_{m,app} = K_M \frac{1 + \frac{[I]}{K_i}}{1 + \frac{[I]}{\alpha K_i}}$$

$$V_{max,app} = \frac{V_{max}}{1 + \frac{[I]}{\alpha K_i}}$$

General method for docking simulations

Interactions of enzymes with compounds were analysed by computational docking using Molecular Operating Environment (MOE) software (Chemical Computing Group ULC, Montreal, Canada). Crystallographic structures of human AChE and human BuChE was obtained from Protein Data Bank (PDB code 4EY6[37] and 4AQD[38], respectively). Protein structures were prepared using Amber10 force field with EHT parameters, R-field solvation model, dielectric constant of 1 for the protein interior and 80 for exterior. Ligand structures were drawn in MOE software, and their energies were minimised using Amber10 force field with EHT parameters for small molecules, using as stop criterion an RMS gradient lower than 0.01 kcal/mol/Å. For the docking calculations: in the placement stage we used the Triangle Matcher algorithm with the London dG scoring scheme. In the refinement stage we kept the receptor rigid and used the GBVI/WSA dG scoring scheme. 2D diagrams were obtained from MOE software and 3D illustrations were obtained using Pymol software.

Antiproliferative activity assays

For the antiproliferative tests, we applied our implementation of the National Cancer Institute (NCI) screening protocol[39]. As a model of human solid tumour cells, we selected the cell lines A549 (non-small cell lung), HBL-100 (breast), HeLa (cervix), SW1573 (non-small cell lung), T-47D (breast), and WiDr (colon). Cell seeding densities, based on the cell line doubling time, were 2500 (A549, HBL-100, HeLa and SW1573) or 5000 (T-47D and WiDr) cells/well. Compounds were initially dissolved in DMSO at 400 times the desired final maximum test concentration. Control cells were exposed to an equivalent concentration of DMSO (0.25% v/v, negative control). Each compound was tested in triplicate at different dilutions ranging from 1 to 100 μM. Drug treatment began on day 1 after sowing. The drug incubation times were 48 h, after which the cells were precipitated with ice-cold TCA (50% w/v) and fixed for 60 min at 4 °C. Then the SRB test was performed. The optical density (OD) of each well was measured at 530 nm using a microplate absorbance reader (PowerWave XS, BioTek Instruments Inc.). Values were corrected for background OD of wells containing medium only[39]. The results were expressed as GI$_{50}$, i.e. the dose that causes 50% growth inhibition after 48 h of exposure.

Synthesis

The synthesis of heterodimers **9a**, **10a**, and **11a** commenced from L-xylose (**14a**), which was converted into 2,3,5-tri-O-benzyl-L-xylo-furanose (**15a**) by following a reported three step procedure (Scheme 2)[40]. The obtained furanose underwent three subsequent chemical modifications including: (1) aldoxime formation, (2) selective O-silylation of the oxime oxygen atom, and (3) mesylation to provide compound **16a**[41] in 78% yield after purification by silica gel chromatography. When **16a** was treated with F⁻ ions it cyclized into nitrone **17a**[42,43] upon loss of the O-silyl group. Tetra-O-benzylated DAB **18a** was obtained in 82% yield when nitrone **17a** was reduced first by sodium borohydride and followed by zinc in acetic acid[44]. In the following step, **18a** underwent N-propargylation to form alkyne **19a** when it was treated with propargyl bromide. This alkyne underwent copper-catalysed azide – alkyne cycloaddition[45] with azides **13a**[46], **13b**[32], and **13c**[32] to form heterodimers **20a**, **21a**, and **22a**, respectively. In the final step,
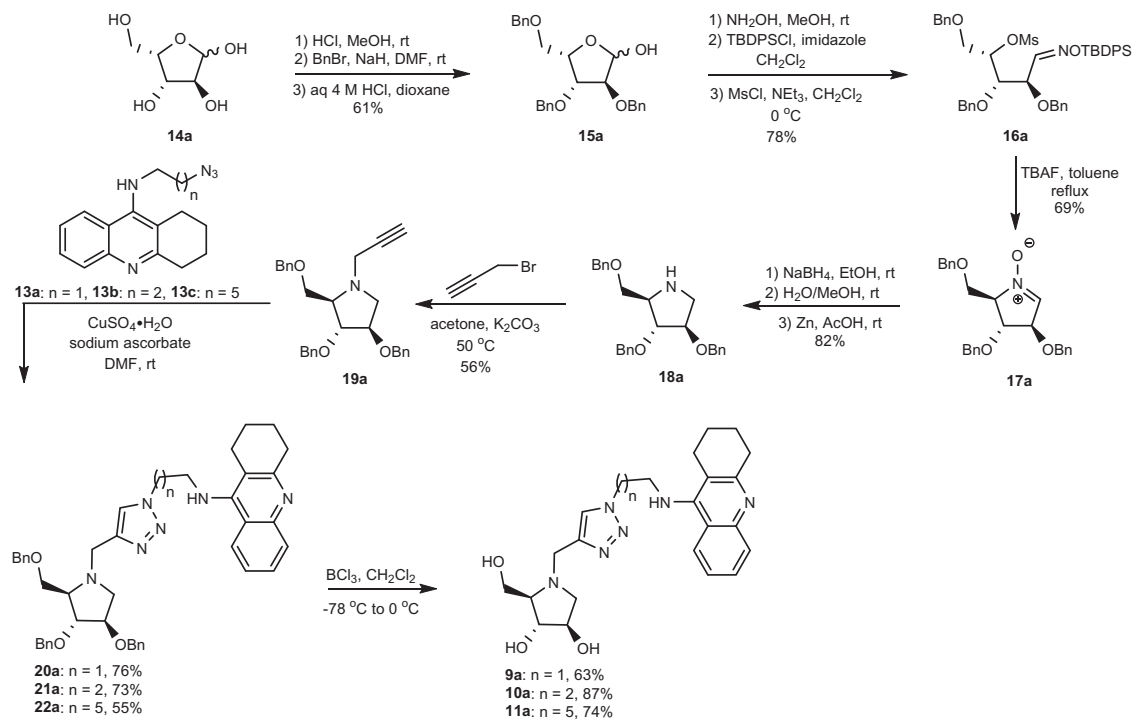
Scheme 2. Synthesis of heterodimers **9a**–**11a**.
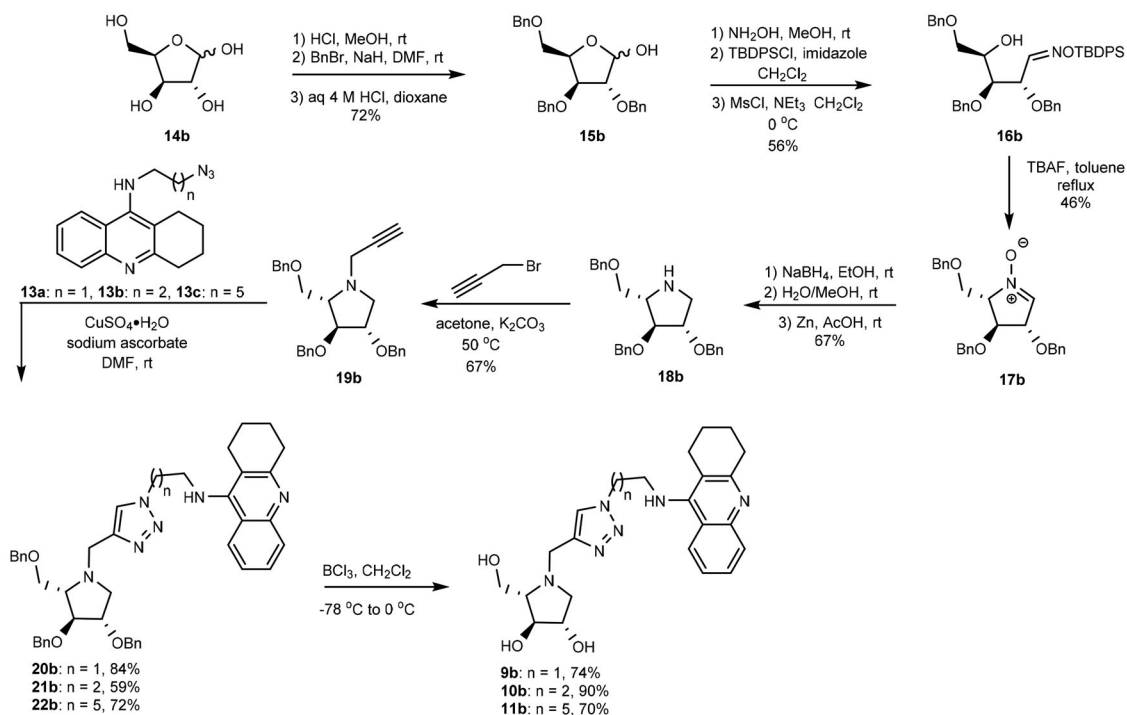
Scheme 3. Synthesis of heterodimers **9b**, **10b**, and **11b**.

Table 1. IC$_{50}$ values for the inhibition of *ee*AcHE and eqBuChE by **9a**, **10a**, and **11a** and with their mirror images **9b**, **10b**, and **11b**.

9a: n = 1, **10a**: n = 2, **11a**: n = 5   **9b**: n = 1, **10b**: n = 2, **11b**: n = 5

	IC$_{50}$ (nM)[a]			
Compound	*ee*AChE[b]	eqBuChE[c]	Enantioselectivity (*ee*AChE)[d]	Enantioselectivity (eqBuChE)[e]
(-)-Galantamine (**2a**)	1300 ± 100	5500 ± 400	–	–
Tacrine	290 ± 2	2.8 ± 0.2	–	–
9a	420 ± 10	96 ± 5	–	–
9b	1480 ± 240	179 ± 25	0.28	0.54
10a	530 ± 30	184 ± 16	–	–
10b	150 ± 38	232 ± 28	3.5	0.79
11a	9.7 ± 1	9.1 ± 0.3	–	–
11b	10.7 ± 0.3	8.1 ± 0.1	0.91	1.1
	$K_i = 19.0 \pm 1.8$ nM $\alpha K_i = 21.9 \pm 7.2$ nM (mixed)	$K_i = 10.0 \pm 2.7$ nM $\alpha K_i = 14.3 \pm 3.3$ nM (mixed)		

[a]Mean ± SD.
[b][S] = 121 μM.
[c][S] = 112 μM.
[d]IC$_{50}$(**Xa**:AChE)/IC$_{50}$(**Xb**:AChE).
[e]IC$_{50}$(**Xa**:BuChE)/IC$_{50}$(**Xb**,BuChE). (K_i: competitive inhibition constant and αK_i: uncompetitive inhibition constant).

heterodimers **20a**, **21a**, and **22a** underwent BCl$_3$ promoted de-*O*-benzylation to generate target compounds **9a**, **10a**, and **11a**, respectively.

The synthesis of **9b**, **10b**, and **11b** were performed in the same way as for **9a**, **10a**, and **11a** by replacing L-xylose (**14a**) with D-xylose (**14b**) in the first step (Scheme 3).
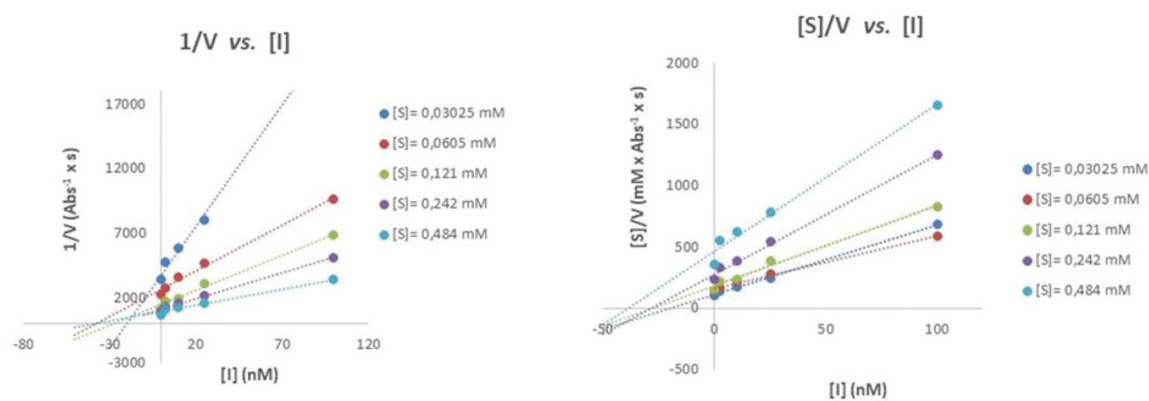
Figure 3. Cornish-Bowden plots for analysing the inhibition mode of *ee*AChE by **11b**.

Figure 4. (a) Docking simulations for the interactions in the **11a**-*rh*AChE complex. (b) Three-dimensional structure of *rh*AChE showing the binding mode of compound **11a**. The residues, Ser203, His447, and Glu334 corresponding to the catalytic triad are depicted in sticks.
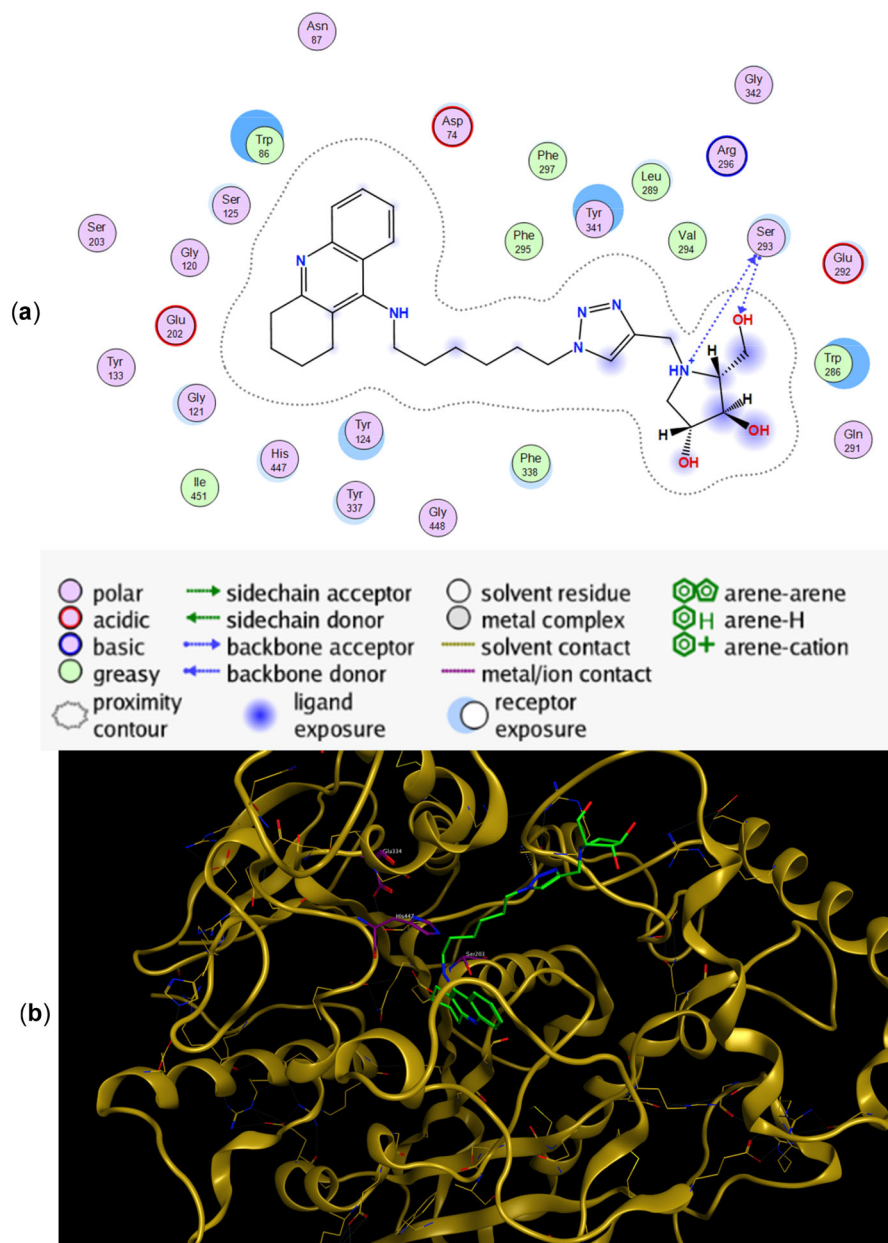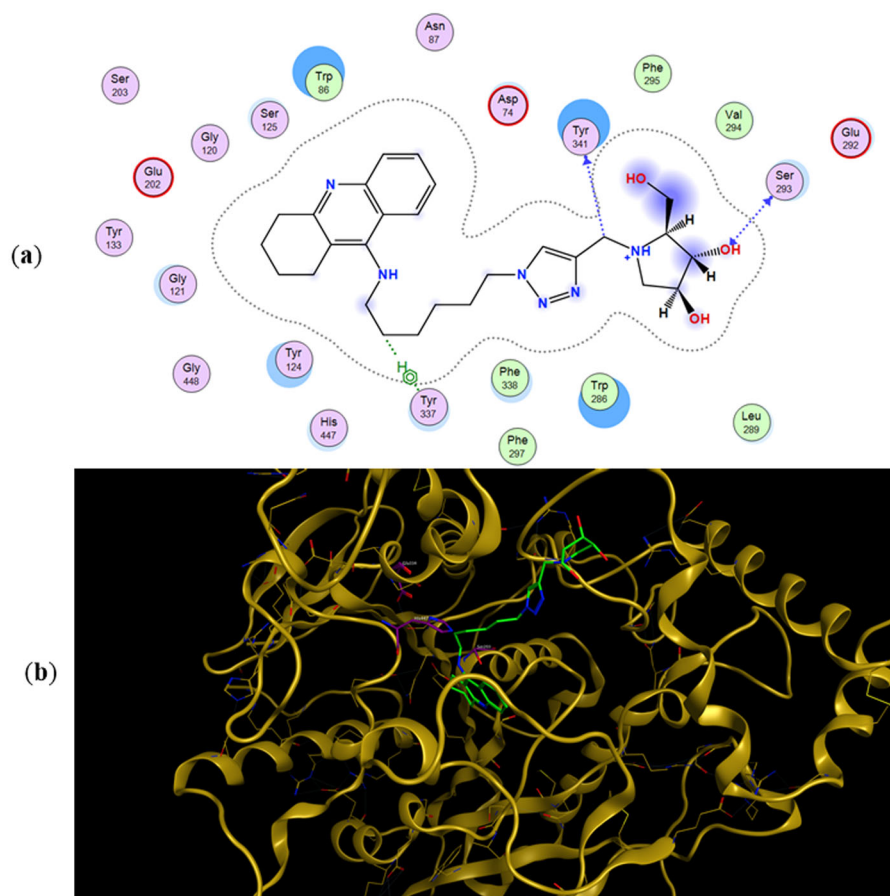
Figure 5. (a) Docking simulations for the interactions in the **11b**-*rh*AChE complex. (b) Three-dimensional structure of *rh*AChE showing the binding mode of compound **11b**. The residues, Ser203, His447, and Glu334 corresponding to the catalytic triad are depicted in sticks.

ChE inhibitory testing

The minimum inhibitory concentrations of the enantiomeric pairs **9a** and **9b**, **10a** and **10b**, and **11a** and **11b** required to reach 50% inhibition (IC_{50}) of *ee*AChE and eqBuChE are presented in Table 1. A minor modification of the Ellman assay was used in order to measure the IC_{50} values[35]. The test series included (-)-galantamine (**2a**) and tacrine as positive references.

Both series of stereoisomers **9a**–**11a** (incorporating a DAB moiety) and **9b**–**11b** (incorporating a LAB moiety) displayed IC_{50} values from the submicromolar concentration range down to the nanomolar concentration range for the inhibition of *ee*AChE and eqBuChE. The only exception was **9b**, which exhibits a IC_{50} value of 1480 nM for the inhibition of *ee*AChE. Thereby, **9b** was the only compound in the testing series that is a less potent AChE inhibitor than (-)-galantamine, which is in in current use against AD[47].

The length of the linker between the tacrine ring and iminosugar moiety had a significant impact on the inhibition potency of both *ee*AChE and eqBuChE in which a longer linker provided higher inhibition potencies. This was demonstrated by the result that **11a** ($n = 5$, $IC_{50} = 9.7$ nM against *ee*AChE) is a *ca.* 43-fold more potent *ee*AChE inhibitor than **9a** ($n = 1$, $IC_{50} = 420$ nM against *ee*AChE) and a 55-fold more potent *ee*AChE inhibitor than **10a** ($n = 2$, $IC_{50} = 530$ nM against *ee*AChE). A similar trend was observed when the enantiomer of **11a**, namely, **11b** ($n = 5$, 10.7 nM against *ee*AChE) was compared with **9b** ($n = 1$, 1480 nM against *ee*AChE) and **10b** ($n = 2$, 150 nM against *ee*AChE) for the inhibition of the same enzyme as **11b** is a *ca.* 138- and 14-fold stronger inhibitor than **9b** and **10b**, respectively. Six CH_2-groups

between the 1,2,3-triazole and tacrine moiety was also most favourable for the inhibition of eqBuChE as **11a** ($n = 5$, $IC_{50} = 9.1$ nM against eqBuChE) is a roughly 11-fold stronger inhibitor than **9a** ($n = 1$, $IC_{50} = 96$ nM against eqBuChE) and a 20-fold stronger inhibitor than **10a** ($n = 2$, $IC_{50} = 184$ nM against eqBuChE). Likewise, **11b** ($n = 5$, $IC_{50} = 8.1$ nM against eqBuChE) is a 22- and 29-fold stronger eqBuChE inhibitor than **9b** ($n = 1$, $IC_{50} = 179$ nM against eqBuChE) and **10b** ($n = 2$, $IC_{50} = 232$ μM against eqBuChE), respectively.

No obvious enantioselectivity of *ee*AChE and eqBuChE was observed for the three pairs of enantiomeric inhibitors included in this study. In addition, no preferential inhibitory activity trend was found for the enantiomers incorporating a DAB or LAB moiety. For instance, **9a** is a *ca.* 4-fold more potent *ee*AChE inhibitor than its enantiomer **9b**, whereas **10b** is a *ca.* 4-fold more potent *ee*AChE inhibitor than its enantiomer **10a**. For the enantiomeric pair **11a** and **11b**, we observed essentially equal *ee*AChE inhibitory activities. These observations indicate that the impact on the *ee*AChE inhibitory potency of our heterodimers by switching between a DAB and LAB moiety is small compared to the contribution from the tacrine ring.

The inhibition modes of *ee*AChE and eqBuChE by heterodimer **11b** were investigated by using the Cornish-Bowden method, that is, by creating two plots (1/V *vs.* [I] and [S]/V *vs.* [I]) for the inhibition of both enzymes (Figure 3). The two plots for the inhibition of each enzyme included a point of intersection at different [I]-coordinates, which implies that **11b** is a mixed inhibitor of both enzymes[47]. The competitive inhibition constant, K_i, and uncompetitive inhibition constant, αK_i, for *ee*AChE by **11b** is 19.0 ± 1.8 nM and

21.9 ± 7.2 nM, respectively. The inhibition constants of eqBuChE are $K_i = 10.0 \pm 2.7$ nM and $\alpha K_i = 14.3 \pm 3.3$ nM. The mixed inhibition modes of eeAChE and eqBuChE by **11b** were interpreted to indicate that **11b** behaves as a dual binding site inhibitor of both enzymes; it is tempting to think that **11b** binds simultaneously to the active site and PAS of both eeAChE and eqBuChE. However, in this context it is worth mentioning that the architecture of PAS in the two enzymes is different as it is richer on aromatic amino acid residues in eeAChE[48,49], which allow formation of π–π interactions and cation–π interactions with ligands[50].

Table 2. Binding energies for **9a**, **9b**, **10a**, **10b**, **11a**, and **11b** to rhAChE and hBuChE.

Compound	Binding energies (kcal/mol)	
	rhAChE	hBuChE
9a	−9.25	−8.83
9b	−9.05	−8.94
10a	−9.52	−9.53
10b	−8.91	−9.44
11a	−10.45	−9.57
11b	−9.92	−9.67

Modelling studies

The preferred binding poses for enantiomers **11a** and **11b** in recombinant human acetylcholinesterase (rhAChE) are presented in Figure 4 and Figure 5, respectively, whereas the preferred binding poses for the enantiomeric pairs **9a** and **9b**, and **10a** and **10b** are presented in Figure SI2 and Figure SI3, respectively. A common trend for all energetically preferred binding poses is that the tacrine moiety and the iminosugar moiety bind to the active site and PAS, respectively. Such preferred binding pose is not very surprising given that X-ray analysis has shown that tacrine is bound to the active site of AChE[51].

Hydrogen bonding interactions between one of the hydroxyl groups of the iminosugar moiety and Ser293 in rhAChE are observed in both **11a** (Figure 4) and **11b** (Figure 5). Interestingly, the protonated imino group of **11a** showed another hydrogen bond with the same Ser293, a feature not observed in **11b**. This helps explain the lower binding energy for **11a** (−10.45 kcal/mol) compared to its antipode **11b** (−9.92 kcal/mol) (Table 2). Slight differences in binding energies were also observed between enantiomers **9a** and **9b** (−9.25 kcal/mol for **9a** vs. −9.05 kcal/mol for **9b**) and between **10a** and **10b** (−9.52 kcal/mol for **10a** vs. −8.91 kcal/mol for **10b**) when they are bound to rhAChE. The
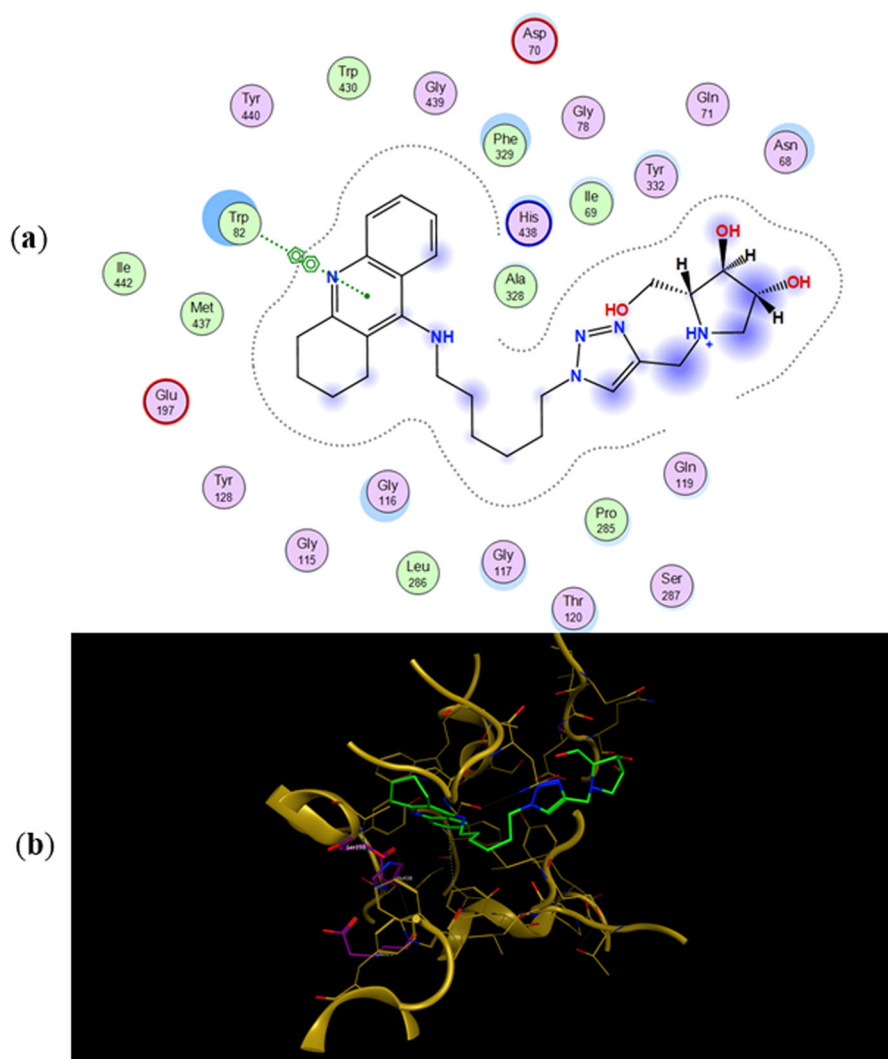

Figure 6. (a) Docking simulations for the interactions in the **11a**-hBuChE complex. (b) Three-dimensional structure of hBuChE showing the binding mode of compound **11a**. The residues, Ser198, His438 and Glu325, corresponding to the catalytic triad are depicted in sticks.

Figure 7. (a) Docking simulations for the interactions in the **11b**-*h*BuChE complex. (b) Three-dimensional structure of *h*BuChE showing the binding mode of compound **11b**. The residues, Ser198, His438, and Glu325, corresponding to the catalytic triad are depicted in sticks.
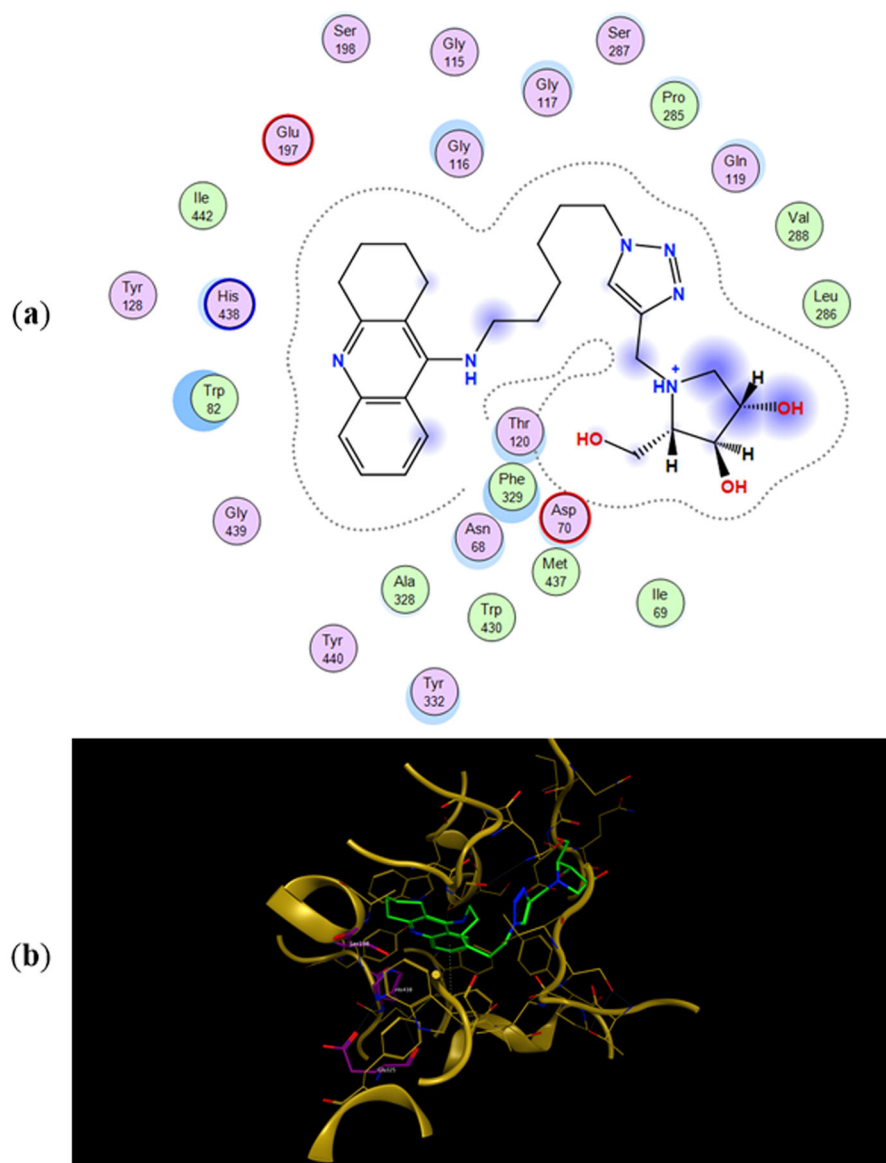
Table 3. Antiproliferative activity (GI_{50}) of **9a**, **9b**, **10a**, **10b**, **11a**, and **11b** against human cancer cells.

Compound	GI₅₀ (µM)					
	A549	HBL-100	HeLa	SW1573	T-47D	WiDr
11a	94 ± 9.6	>100	93 ± 12	>100	>100	>100
11b	84 ± 28	>100	>100	97 ± 5.4	>100	>100

hydroxyl groups of **9a** showed interactions with Tyr341 and Arg296 meanwhile there is an arene cation interaction between one of the hydroxyl groups in **9b** and Trp286 (Figure SI2). Hydrogen bond interaction between Ser293 and the iminosugar moiety is observed for **10a** but is lacking in its antipode **10b** (Figure SI3).

We found that our measured IC_{50} values (Table 1) for the inhibition of *ee*AChE by **11a** and **11b** are in agreement with the calculated binding energies (Table 2), which predict **11a** and **11b** to possess the highest affinity for the enzyme. However, IC_{50} is not a true measure of binding affinity of a ligand to an enzyme[52], which

explains why the calculated binding energies in Table 2 fail in predicting the relative IC_{50} values for the inhibition of *ee*AChE by the heterodimers (**9a**–**11a** and **9b**–**11b**) in our series.

The most energetically favourable binding poses of enantiomers **11a** and **11b** to human butyrylcholinesterase (*h*BuChE) are presented in Figure 6 and Figure 7, respectively. The preferred binding poses of the enantiomeric pairs **9a** and **9b**, and **10a** and **10b** to the same enzyme are presented in Figures SI5 and SI6, respectively. The number of CH_2-groups between the tacrine ring and 1,2,3-triazole ring appears to control whether the iminosugar moiety is bound to the active site or PAS. In fact, the tacrine ring of **9a**, **9b**, **11a**, and **11b** is accommodated in the active site whereas their iminosugar moiety is bound to PAS. For heterodimers **10a** and **10b** the binding scenarios are different, as the tacrine ring is accommodated in PAS and the iminosugar moiety in the active site. As for the inhibition of *ee*AChE, even though the calculated binding energies in Table 2 predict **11a** and **11b** to be the most potent BuChE inhibitors, they fail in predicting the relative IC_{50} values for the whole testing series.

Antiproliferative activity

Antiproliferative activity of our heterodimers was investigated for six cancer cell lines including A549, HBL-100, HeLa, SW1573, T-47D and WiDr. The inhibition of cancer cell growth by each heterodimer is expressed in concentration of heterodimer required to lower the cell growth by 50% (GI_{50}). The antiproliferative activity of a compound is only significant when $GI_{50} < 100\,\mu M$. The measured GI_{50} values demonstrated that those heterodimers with two CH_2-groups (**9a** and **9b**) and three CH_2-groups (**10a** and **10b**) between the tacrine and 1,2,3-triazole rings display no significant antiproliferative activity ($GI_{50} > 100\,\mu M$). **11a** and **11b** on the other hand that contain six CH_2-groups between the tacrine and 1,2,3-triazole rings display GI_{50} values below $100\,\mu M$ for the inhibition of A549 cancer cell growth (Table 3). In addition, **11a** and **11b** display weak but significant inhibition of cell growth of HeLa and SW1573 cancer cells, respectively.

Conclusions

In contrast to the enantiomeric pairs **1a** and **1b** of huperzine, **2a** and **2b** of galantamine, and **3a** and **3b** of physostigmine, our enantiomeric pairs **9a** and **9b**, **10a** and **10b**, and **11a** and **11b** of iminosugar-tacrine heterodimers displayed low enantioselectivity (<4) for the inhibition of *ee*AChE and *eq*BuChE. The following three observations: (1) **9a** is a *ca.* 3.5-fold stronger *ee*AChE inhibitor than **9b**, (2) **10a** is a *ca.* 3.5-fold less potent *ee*AChE inhibitor than **10b**, and (3) **11a** and **11b** are essentially equipotent *ee*AChE inhibitors, show that *ee*AChE exhibits no consequent preference for any of the enantiomeric heterodimers, which include a DAB or LAB moiety. These observations can either be interpreted as the tacrine moiety contributes much more to the *ee*AChE inhibitory potencies than the DAB or LAB moieties or that the LAB and DAB moieties have similar contribution to the inhibition potencies when they are connected to a tacrine ring. However, the latter interpretation is to some extent contradicted by the modelling studies, which show that the DAB and LAB moieties display different interaction modes with the enzymes.

Like in our earlier studies when we connected an iminosugar to a tacrine ring to obtain ChE inhibitors of type **7** in Figure 2[32], heterodimers **11a** and **11b** with the longest linkers exhibited the highest inhibition potencies. From modelling studies for the binding to BuChE, it appeared that the length of the linker between the tacrine ring and DAB or LAB moiety controls whether the tacrine ring binds to the active site of PAS. On the other hand, because the trend of the measured IC_{50} values do not parallel the calculated binding energies, it is possible that the title compounds are not bound in their most energetically favourable poses when they inhibit the enzymes in our testing series.

Author contributions

Conceptualisation, E.L.; methodology, I.C.V. and Ó.L.; funding acquisition, E.L, M.O.S., Ó.L., J.M.P., and J.G.F.B.; investigation, E.L, I.C.V, A.P., M.X.F., and Ó.L.; project administration, E.L.; resources, E.L., Ó.L., M.O.S., J.M.P., and J.G.F.B.; supervision, E.L. and M.O.S.; writing – original draft, E.L., I.C.V.; writing – review & editing, E.L., Ó.L., I.C.V., M.O.S., J.M.P., and J.G.F.B.
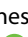
Disclosure statement

The authors report no conflicts of interest.

ORCID

Óscar López http://orcid.org/0000-0003-2896-6993
Adrián Puerta http://orcid.org/0000-0002-7975-1960
Miguel X. Fernandes http://orcid.org/0000-0002-1840-616X
José M. Padrón http://orcid.org/0000-0001-6268-6552
José G. Fernández-Bolaños http://orcid.org/0000-0003-1499-0650
Magne O. Sydnes http://orcid.org/0000-0001-9413-6969
Emil Lindbäck http://orcid.org/0000-0001-5809-7368

References

1. Ramsay RR, Tipton KF. Assessment of enzyme inhibition: a review with examples from the development of monoamine oxidase and cholinesterase inhibitory drugs. Molecules. 2017;22(7):1192.
2. Fokkens J, Klebe G. A simple protocol to estimate differences in protein binding affinity for enantiomers without prior resolution of racemates. Angew Chem Int Ed Engl. 2006; 45(6):985–989.
3. Mentel M, Blankenfeldt W, Breinbauer R. The active site of an enzyme can host both enantiomers of a racemic ligand simultaneously. Angew Chem Int Ed Engl. 2009;48(48): 9084–9087.
4. Brooks WH, Guida WC, Daniel KG. The significance of chirality in drug design and development. Curr Top Med Chem. 2011;1:760–770.
5. McKinney M, Miller JH, Yamada F, Tuckmantel W, Kozikowski AP. Potencies and stereoselectivities of enantiomers of huperzine A for inhibition of rat cortical acetylcholinesterase. Eur J Pharmacol. 1991;203(2):303–305.
6. Zhang HY, Liang YQ, Tang XC, He XC, Bai DL. Stereoselectivities of enantiomers of huperzine A in protection against beta-amyloid(25-35)-induced injury in PC12 and NG108-15 cells and cholinesterase inhibition in mice. Neurosci Lett. 2002;317(3):143–146.
7. Anand P, Singh B. A review on cholinesterase inhibitors for Alzheimer's disease. Arch Pharm Res. 2013;36(4):375–399.
8. Zangara A. The psychopharmacology of huperzine A: an alkaloid with cognitive enhancing and neuroprotective properties of interest in the treatment of Alzheimer's disease. Pharmacol Biochem Behav. 2003;75(3):675–686.
9. Orhan IE, Orhan G, Gurkas E. An overview on natural cholinesterase inhibitors–a multi-targeted drug class–and their mass production. Mini Rev Med Chem. 2011;11(10):836–842.
10. Dvir H, Jiang HL, Wong DM, Harel M, Chetrit M, He XC, Jin GY, Yu GL, Tang XC, Silman I, et al. X-ray structures of *Torpedo californica* acetylcholinesterase complexed with (+)-huperzine A and (-)-huperzine B: structural evidence for

an active site rearrangement. Biochemistry. 2002;4: 10810–10818.

11. Sussman JL, Harel M, Frolow F, Oefner C, Goldman A, Toker L, Silman I. Atomic structure of acetylcholinesterase from *Torpedo californica*: a prototypic acetylcholine-binding protein. Science. 1991;253(5022):872–879.

12. Sramek JJ, Frackiewicz EJ, Cutler NR. Review of the acetylcholinesterase inhibitor galanthamine. Expert Opin Investig Drugs. 2000;9(10):2393–2402.

13. Greenblatt HM, Kryger G, Lewis T, Silman I, Sussman JL. Structure of acetylcholinesterase complexed with (-)-galanthamine at 2.3 A resolution. FEBS Lett. 1999;463(3):321–326.

14. Kimura H, Kawai T, Hamashima Y, Kawashima H, Miura K, Nakaya Y, Hirasawa M, Arimitsu K, Kajimoto T, Ohmomo Y, et al. Synthesis and evaluation of (–)- and (+)-[^{11}C]galanthamine as PET tracers for cerebral acetylcholinesterase imaging. Bioorg Med Chem. 2014;22(1): 285–291.

15. Brossi A, Schönenberger B, Clark OE, Ray R. Inhibition of acetylcholinesterase from electric eel by (-)-and (+)-physostigmine and related compounds. FEBS Lett. 1986;201(2): 190–192.

16. Triggle DJ, Mitchell JM, Filler R. The pharmacology of physostigmine. CNS Drug Rev. 1998;4(2):87–136.

17. McNaught AD. Nomenclature of carbohydrates (IUPAC recommendations 1996). Pure Appl Chem. 1996;68(10): 1919–2008.

18. Horne G, Wilson FX, Tinsley J, Williams DH, Storer R. Iminosugars past, present and future: medicines for tomorrow. Drug Discov Today. 2011;16(3-4):107–118.

19. Lillelund VH, Jensen HH, Liang X, Bols M. Recent developments of transition-state analogue glycosidase inhibitors of non-natural product origin. Chem Rev. 2002;102(2):515–553.

20. Asano N, Nash RJ, Molyneux RJ, Fleet GWJ. Sugar-mimic glycosidase inhibitors: natural occurrence, biological activity and prospects for therapeutic application. Tetrahedron Asymmetry. 2000;11:49–58.

21. Sánchez-Fernández EM, Gonçalves-Pereira R, Rísquez-Cuadro R, Plata GB, Padrón JM, García Fernández JM, Ortiz Mellet C. Influence of the configurational pattern of sp(2)-iminosugar pseudo N-, S-, O- and C-glycosides on their glycoside inhibitory and antitumor properties. Carbohydr Res. 2016;429: 113–122.

22. Sánchez-Fernández EM, García-Hernández R, Gamarro F, Arroba AI, Aguilar-Diosdado M, Padrón JM, García Fernández JM, Ortiz Mellet C. Synthesis of sp^2-iminosugar selenoglycolipids as multitarget drug candidates with antiproliferative, leishmanicidal and anti-inflammatory properties. Molecules. 2021;26(24):7501.

23. Sugimoto S, Nakajima H, Kosaka K, Hosoi H. Review: miglitol has potential as a therapeutic drug against obesity. Nutr Metab. 2015;12:51.

24. Stirnemann J, Belmatoug N, Camou F, Serratrice C, Froissart R, Caillaud C, Levade T, Astudillo L, Serratrice J, Brassier A, et al. A review of Gaucher disease pathophysiology, clinical presentation and treatments. IJMS. 2017;18(2):441.

25. Sunder-Plassmann G, Schiffmann R, Nicholls K. Migalastat for the treatment of Fabry disease. Expert Opin Orphan Drugs. 2018;6:303–309.

26. Noel A, Ingrand S, Barrier L. Anti-amyloidogenic effects of glycosphingolipid synthesis inhibitors occur independently of ganglioside alterations. Mol Cell Neurosci. 2016;75:63–70.

27. Macdonald IR, Martin E, Rosenberry TL, Darvesh S. Probing the peripheral site of human butyrylcholinesterase. Biochemistry. 2012;51(36):7046–7053.

28. Gloster TM, Meloncelli P, Stick RV, Zechel D, Vasella A, Davies GJ. Glycosidase inhibition: an assessment of the binding of 18 putative transition-state mimics. J Am Chem Soc. 2007;129(8):2345–2354.

29. Decroocq C, Stauffert F, Pamlard O, Oulaïdi F, Gallienne E, Martin OR, Guillou C, Compain P. Iminosugars as a new class of cholinesterase inhibitors. Bioorg Med Chem Lett. 2015; 25(4):830–833.

30. Olsen JI, Plata GB, Padrón JM, López Ó, Bols M, Fernández-Bolaños JG. Selenoureido-iminosugars: a new family of multitarget drugs. Eur J Med Chem. 2016;123:155–160.

31. Ahuja-Casarín AI, Merino-Montiel P, Vega-Baez JL, Montiel-Smith S, Fernandes MX, Lagunes I, Maya I, Padrón JM, López Ó, Fernández-Bolaños JG. Tuning the activity of iminosugars: novel *N*-alkylated deoxynojirimycin derivatives as strong BuChE inhibitors. J Enzyme Inhib Med Chem. 2021;36(1): 138–146.

32. de Santana QLO, Santos Evangelista TC, Imhof P, Baptista Ferreira S, Fernández-Bolaños JG, Sydnes MO, Lopéz Ó, Lindbäck E. Tacrine-sugar mimetic conjugates as enhanced cholinesterase inhibitors. Org Biomol Chem. 2021;19(10): 2322–2337.

33. Santos Evangelista TC, López Ó, Puerta A, Fernandes MX, Baptista Ferreira S, Padrón JM, Fernández-Bolaños JG, Sydnes MO, Lindbäck E. A hybrid of 1-deoxynojirimycin and benzotriazole induces preferential inhibition of butyrylcholinesterase (BuChE) over acetylcholinesterase (AChE). J Enzyme Inhib Med Chem. 2022;37(1):2395–2402.

34. Janockova J, Korabecny J, Plsikova J, Babkova K, Konkolova E, Kucerova D, Vargova J, Koval J, Jendzelovsky R, Fedorocko P, et al. In vitro investigating of anticancer activity of new 7-MEOTA-tacrine heterodimers. J Enzyme Inhib Med Chem. 2019;34(1):877–897.

35. Ellman GL, Courtney KD, Andres V Jr, Feather-Stone RM. A new and rapid colorimetric determination of acetylcholinesterase activity. Biochem Pharmacol. 1961;7:88–95.

36. Moutayakine A, Marques C, López Ó, Bagetta D, Leitzbach L, Hagenow S, Carreiro EP, Stark H, Alcaro S, Fernández-Bolaños JG, et al. Evaluation of chromane derivatives: promising privileged scaffolds for lead discovery within Alzheimer's disease. Bioorg Med Chem. 2022;68:116807.

37. Lagunes I, Martín-Batista E, Silveira-Dorta G, Fernandes MX, Padrón JM. Differential mechanism of action of the CK1ε inhibitor GSD0054. J Mol Clin Med. 2018;1:77–84.

38. Cheung J, Rudolph MJ, Burshteyn F, Cassidy MS, Gary EN, Love J, Franklin MC, Height JJ. Structures of human acetylcholinesterase in complex with pharmacologically important ligands. J Med Chem. 2012;55(22):10282–10286.

39. Brazzolotto X, Wandhammer M, Ronco C, Trovaslet M, Jean L, Lockridge O, Renard PY, Nachon F. Human butyrylcholinesterase produced in insect cells: huprine-based affinity purification and crystal structure. FEBS J. 2012;279(16): 2905–2916.

40. Santos Evangelista TC, Lopéz Ó, Sydnes MO, Fernández-Bolaños JG, Baptista Ferreira S, Emil Lindbäck E. Bicyclic 1-azafagomine derivatives: synthesis and glycosidase inhibitory testing. Synthesis. 2019;51(21):4066–4077.

41. Desvergnes S, Py S, Vallée Y. Total synthesis of (+)-hyacinthacine A$_2$ based on SmI$_2$-induced nitrone umpolung. J Org Chem. 2005;70(4):1459–1462.

42. Carmona AT, Whigtman RH, Robina I, Vogel P. Synthesis and glycosidase inhibitory activity of 7-deoxycasuarine. HCA. 2003;86(9):3066–3073.

43. Cardona F, Faggi E, Liguori F, Cacciarini M, Goti A. Total syntheses of hyacinthacine A2 and 7-deoxycasuarine by cycloaddition to a carbohydrate derived nitrone. Tetrahedron Lett. 2003;44(11):2315–2318.

44. D'Adamio G, Matassini C, Parmeggiani C, Catarzi S, Morrone A, Goti A, Paoli P, Cardona F. Evidence for a multivalent effect in inhibition of sulfatases involved in lysosomal storage disorders (LSDs). RSC Adv. 2016;6(69):64847–64851.

45. Breugst M, Reissig HU. The Huisgen reaction: milestones of the 1,3-dipolar cycloaddition. Angew Chem Int Ed Engl. 2020;59(30):12293–12307.

46. Oukoloff K, Coquelle N, Bartolini M, Naldi M, Le Guevel R, Bach S, Josselin B, Ruchaud S, Catto M, Pisani L, et al. Design, biological evaluation and X-ray crystallography of nanomolar multifunctional ligands targeting simultaneously acetylcholinesterase and glycogen synthase kinase-3. Eur J Med Chem. 2019;168:58–77.

47. Cornish-Bowden A. A simple graphical method for determining the inhibition constants of mixed, uncompetitive and non-competitive inhibitors. Biochem J. 1974;137(1):143–144.

48. Rosenberry TL, Brazzolotto X, Macdonald IR, Wandhammer M, Trovaslet-Leroy M, Darvesh S, Nachon F. Comparison of the binding of reversible inhibitors to human butyrylcholinesterase and acetylcholinesterase: a crystallographic, kinetic and calorimetric study. Molecules. 2017;22(12):2098.

49. Radić Z, Pickering NA, Vellom DC, Camp S, Taylor P. Three distinct domains in the cholinesterase molecule confer selectivity for acetyl- and butyrylcholinesterase inhibitors. Biochemistry. 1993;32(45):12074–12084.

50. Barak D, Kronman C, Ordentlich A, Ariel N, Bromberg A, Marcus D, Lazar A, Velan B, Shafferman A. Acetylcholinesterase peripheral anionic site degeneracy conferred by amino acid arrays sharing a common core. J Biol Chem. 1994;269(9):6296–6305.

51. Harel M, Schalk I, Ehret-Sabatier L, Bouet F, Goeldner M, Hirth C, Axelsen PH, Silman I, Sussman JL. Quaternary ligand binding to aromatic residues in the active-site gorge of acetylcholinesterase. Proc Natl Acad Sci U S A. 1993;90(19): 9031–9035.

52. Holdgate G, Meek T, Grimley R. Mechanistic enzymology in drug discovery: a fresh perspective. Nat Rev Drug Discov. 2018;17(2):115–132.